# BrainAligner: 3D registration atlases of *Drosophila* brains

Hanchuan Peng[1], Phuong Chung[1], Fuhui Long[1], Lei Qu[1], Arnim Jenett[1], Andrew M Seeds[1], Eugene W Myers[1,2] & Julie H Simpson[1,2]



**Analyzing *Drosophila melanogaster* neural expression patterns in thousands of three-dimensional image stacks of individual brains requires registering them into a canonical framework based on a fiducial reference of neuropil morphology. Given a target brain labeled with predefined landmarks, the BrainAligner program automatically finds the corresponding landmarks in a subject brain and maps it to the coordinate system of the target brain via a deformable warp. Using a neuropil marker (the antibody nc82) as a reference of the brain morphology and a target brain that is itself a statistical average of data for 295 brains, we achieved a registration accuracy of 2 μm on average, permitting assessment of stereotypy, potential connectivity and functional mapping of the adult fruit fly brain. We used BrainAligner to generate an image pattern atlas of 2,954 registered brains containing 470 different expression patterns that cover all the major compartments of the fly brain.**

An adult *Drosophila* brain has about 100,000 neurons with cell bodies at the outer surface and neurites extending into the interior to form the synaptic neuropil. Specific types of neurons can be labeled using antibody detection[1] or genetic methods such as the upstream activating sequence–*GAL4* system[2], in which each *GAL4* line drives expression of a fluorescent protein reporter in a different subpopulation of neurons. Computationally registering, or aligning, images of fruit fly brains in three dimensions is useful in many ways. First, automated three-dimensional (3D) alignment of multiple identically labeled brains allows quantitative assessment of stereotypy: how much the expression pattern or the shape of identified neurons varies between individuals. Second, aligning brains that have different antibody or *GAL4* patterns reveals areas of overlapping or distinctive expression that might be selected for genetic intersectional strategies[3]. Third, comparison of aligned neural expression patterns suggests potential neuronal circuit connectivity. Fourth, aligning images of a large collection of *GAL4* lines gives an estimate of how extensively they cover different brain areas. Finally, for behavioral screens that disrupt neural activity in parts of the brain using *GAL4* collections, accurate alignment of images is a prerequisite for detecting anatomical features in brains that correlate with behavior phenotypes.

Earlier 3D image registration approaches[4–6] have used surface- or landmark-based alignment modules of the commercial 3D visualization software Amira (Visage Imaging) to align sample specimens to a template. The major disadvantages of these approaches are the huge amount of time needed for a user to manually segment the surfaces or to define the landmarks in each subject brain and the potential for human error.

The earliest and most relevant parallel line of research for automated alignment is for 2D or 3D biomedical images such as computed tomography and magnetic resonance human brain scans[7–9], and for 2D mouse brain *in situ* hybridization images as part of the Allen Brain Atlas project[10]. Previous efforts to automatically register images of the fruit fly nervous system based on image features include work on adult brains[11,12], adult ventral nerve cord and larval nervous system[13]. In our comparison (**Supplementary Note 1**) of several widely used methods for registration[11–16], all methods yielded unsatisfactory alignments at a rate that make them unsuitable for use in a pipeline that involves thousands of high-resolution 3D laser scanning microscope images of *Drosophila* brains.

In this study we developed an automatic registration program, BrainAligner, for *Drosophila* brains and used it to align 3D laser scanning microscope images of thousands of brains with different neuronal expression patterns. Our algorithm combines several existing approaches into a new strategy based on reliably detecting landmarks in images. BrainAligner is hundreds of times faster than several competitive methods and automatically assesses alignment accuracy with a quality score. We validated alignment accuracy using biological ground truth represented by 'coexpression'. We used BrainAligner to assemble a preliminary 3D *Drosophila* brain atlas, for which we assessed the stereotypy of neurite tract patterns throughout a *Drosophila* brain.

## RESULTS

### BrainAligner

BrainAligner registers 3D images of adult *Drosophila* brain into a common coordinate system (**Fig. 1**). We dissected brains that expressed enhanced GFP (EGFP) in various neural subsets and labeled them with an antibody to EGFP (**Fig. 1a**,**b**); this was the pattern channel. We also labeled brains with nc82, an antibody that

[1]Janelia Farm Research Campus, Howard Hughes Medical Institute, Ashburn, Virginia, USA. [2]These authors contributed equally to this work. Correspondence should be addressed to H.P. (pengh@janelia.hhmi.org).

RECEIVED 15 NOVEMBER 2010; ACCEPTED 21 MARCH 2011; PUBLISHED ONLINE 1 MAY 2011; CORRECTED ONLINE 16 MAY 2011 (DETAILS ONLINE); DOI:10.1038/NMETH.1602

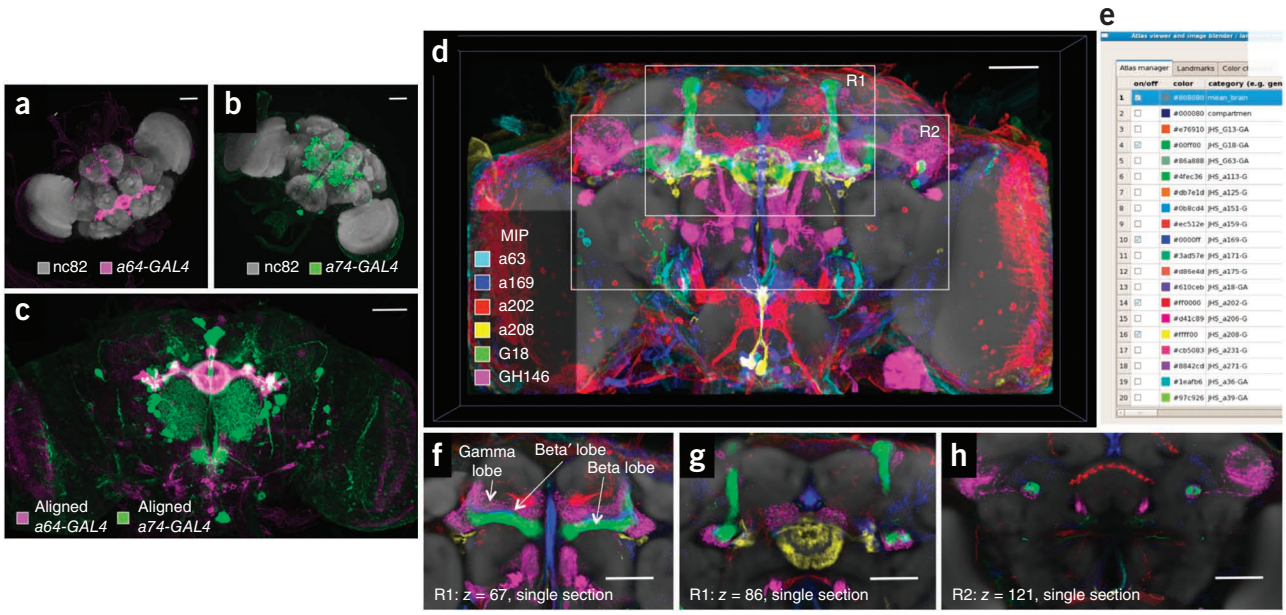


**Figure 1** | BrainAligner registers images of neurons from different brains onto a common coordinate system. (**a**,**b**) Maximum intensity projections of confocal images of enhancer trap *GAL4* lines *a64-GAL4* and *a74-GAL4* brains. Neurons are visualized by membrane-targeted EGFP and brain morphology is visualized by staining with the antibody nc82. (**c**) Aligned and overlaid neuronal patterns shown in **a** and **b**. (**d**) Alignment of many *GAL4* expression patterns. Patterns of interest can be selected and displayed in the common coordinate system. R1 and R2, regions of interest. (**e**) Screenshot from V3D-AtlasViewer software for viewing the 3D pattern atlas. (**f**–**h**) Close-up single-section views of regions marked R1 and R2 in **d** (*z* section numbers are indicated). Scale bars, 50 µm.

detects a ubiquitous presynaptic component and marks the entire synaptic neuropil[17] (**Fig. 1a**,**b**); this was the reference channel. The brains to be registered have different orientations, sizes and morphological deformations that are either biological or introduced in sample preparation. For each subject brain, BrainAligner maps the reference channel to a standardized target brain image using a nonlinear geometrical warp. Using the same transformation, the pattern channel from the subject image is then warped onto the target. Multiple subject images are aligned to a common target so that their patterns can be compared in the same coordinate space (**Fig. 1c** and **Supplementary Video 1**). In this way, we mapped a large collection of *GAL4* patterns into a common framework to identify intersecting expression patterns in various anatomical structures (**Fig. 1d**–**h** and **Supplementary Video 2**).

BrainAligner registers subject to target using a global 3D affine transformation followed by a nonlinear local 3D alignment. For large-scale applications, brains may have different orientations, brightness, sizes, evenness of staining, morphological damage and other types of image noise, which requires our algorithm to be robust. Thus we optimized only the necessary degrees of freedom.

In global alignment, we sequentially optimized the displacement, scaling and rotation parameters of an affine transform from subject to target to maximize the correlation of voxel intensities between two images (**Fig. 2a** and Online Methods). We visually examined the transformed brains after the global alignment and found no transformation errors in over 99% of our samples. The cases with errors typically corresponded to poorly dissected brains that were either damaged structurally or for which excess tissues were present.

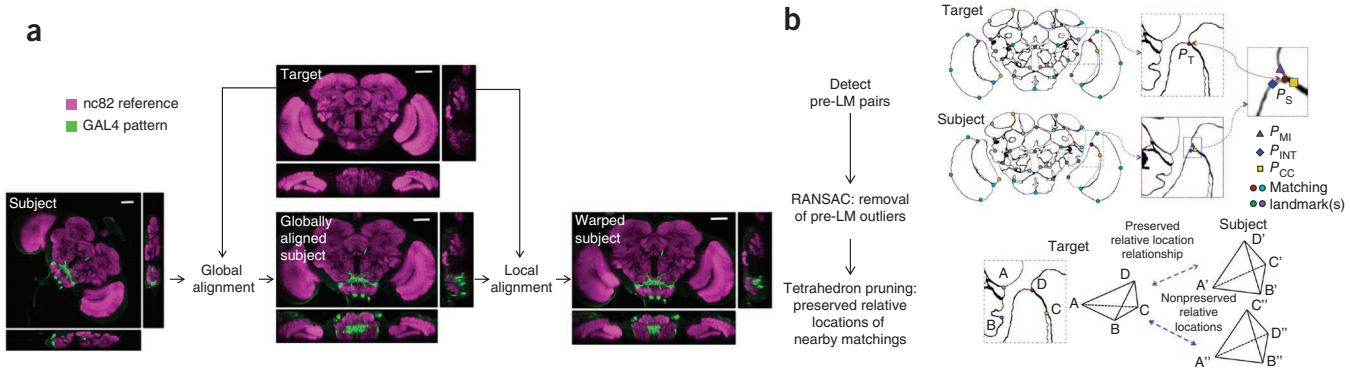


**Figure 2** | Schematic illustration of the BrainAligner algorithm. (**a**) BrainAligner performs a global alignment followed by nonlinear local alignments using landmarks. Scale bars, 50 µm. (**b**) Outline of the RLM algorithm for detecting corresponding feature points in subject and target images. Same-color dots indicate the matching landmarks; $P_T$, a target brain landmark position; $P_S$, a subject brain landmark; and $P_{MI}$, $P_{INT}$ and $P_{CC}$, best matching positions based on mutual information (MI), voxel intensity (INT) and correlation coefficient (CC) of local image patches. In the first insets, only the considered landmark $P_T$ and the best candidate locations are displayed. In the tetrahedron-pruning step, the landmarks in a subject image that clearly violate the relative position relationships of the target are discarded.

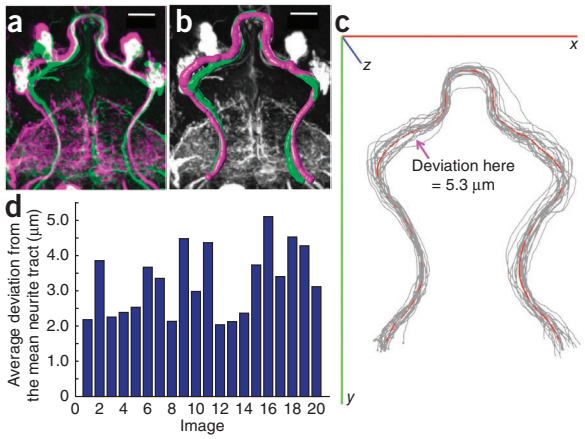


**Figure 3** | Stereotypy of neuronal morphology and reproducibility of *GAL4* expression patterns. (**a**) Two aligned and overlaid examples (magenta and green) of the *a278-GAL4* expression pattern from different brains. (**b**) A 3D reconstruction of the major neurite tracts in **a**. Magenta and green, surface representations of the reconstructed tracts. Gray, GAL4 expression pattern. Scale bars, 20 µm. (**c**) The 3D reconstructed neurite tracts (gray) from 20 aligned *a278-GAL4* images, along with their mean tract model (red; overall average deviation, 3.26 µm). (**d**) Average deviation of the mean tract model from each reconstructed tract.

In the local alignment step, we designed a reliable landmark matching (RLM) algorithm (**Fig. 2b**) to detect corresponding 3D feature points, each of which we called a 'landmark', in every target-subject pair. For the target brain we manually defined 172 landmarks that correspond to the points of high curvature ('corners' or edge points)) of brain compartments as indicated by abrupt image contrast changes in the neuropil labeling. For each target landmark, RLM first searches for its matching landmark in the subject image using two or more independent matching criteria, such as maximizing (i) mutual information[11,18], (ii) inverse intensity difference, (iii) correlation and (iv) similarity of invariant image moments[15], in a small region around the landmark in the target and its potential match in the subject. A match confirmed by a consensus of these criteria is superior to a match based on a single criterion. Therefore, when the best matching locations meeting these criteria are close to each other (<5 voxels apart), RLM reports a preliminary landmark match (pre-LM), which is the site in the 3D bounding box of these best matching locations that gives the maximal product of the individual matching scores. These pre-LMs may violate the smoothness constraint, which states that *in toto* all matching-landmark pairs should be close to a single global affine transform and, locally, that relative location relationships should be preserved. Therefore, RLM uses a random sample consensus algorithm[19] to remove the outliers from the pre-LMs with respect to the global affine transform that produces the fewest outliers. Next, RLM optionally checks the remaining set of pre-LM pairs and detects those violating the relative location relationship in every corresponding tetrahedron formed by three additional neighboring matching points. Pre-LM pairs that clearly create a spatial twist with respect to nearby neighbors are removed. The landmarks that remain are usually highly faithful matching locations and are called reliable landmarks.

We used the reliable landmarks to generate a thin-plate-spline warping field[20] and thus mapped the reference channel of a subject image to the target. We then applied the same warping field derived from the reference channel to the pattern channel. We also optimized BrainAligner's running speed. For instance, to generate the warping field we used hierarchical interpolation (Online Methods) instead of using all image voxels directly, improving the speed 50-fold without visible loss of alignment quality. Typically BrainAligner needs only 40 min on a current single CPU (2.66 GHz Intel Gainestown) to align two images with 1,024 × 1,024 × 256 voxels.

One advantage of RLM is that the percentage of the target landmarks that are automatically reliably matched ($Q_i$) can be used to score how many image features are preserved in the automatic registration. The larger the $Q_i$, the better the respective alignment. We visually inspected the aligned brains and ranked alignment quality using a manual score, $Q_v$ (range = 0–10; the larger, the better). $Q_i$ and $Q_v$ correlated significantly ($P < 10^{-5}$) on 805 randomly selected alignments in the central brain, left optic lobe and right optic lobe (**Supplementary Fig. 1**), suggesting that $Q_i$ is a good indicator of alignment quality. Empirically, for $Q_i > 0.5$ the respective alignment was good; for $Q_i > 0.75$ the alignment was excellent. Low $Q_i$ scores typically corresponded to poorly nc82-stained samples and brains damaged during sample preparation.

Although BrainAligner can be used to align subject brains to any target brain, we prefer to use an optimized 'average' target brain obtained as follows. We first selected one image of a real brain, $T_R$ (**Supplementary Fig. 2**) as the target for an initial alignment for 295 brains that aligned to $T_R$ with $Q_i > 0.75$. We then computed the mean brain image, $T_A$, for the respective local alignments (**Supplementary Fig. 2**). Although $T_A$ was smoother than $T_R$, it preserved detailed information, reflected in the strong correlation between $T_A$ and $T_R$ (**Supplementary Fig. 2**). We used $T_A$ as a new and more meaningful target image for BrainAligner. Compared to the results for $T_R$, this led to 38% and 14% more brains aligning with $Q_i$ scores > 0.7 and > 0.5, respectively, in a dataset of 496 brains (**Supplementary Fig. 3).**

### Assessment of BrainAligner accuracy and biological variance

The variation between individual aligned brains of the same genotype is a combination of biological difference, variation introduced during sample preparation or imaging and alignment error. In a previous study[11], the variance of axon position had been estimated to be ~2.5–4.3 µm in the inner antennal cerebral tract and at its neurite bifurcation point. We addressed a similar question by aligning 20 images of *a278-GAL4;UAS-mCD8-GFP* fly brains to the common target $T_A$. We traced the large neurite bundles in aligned images in three dimensions (**Fig. 3a**,**b**) using V3D-Neuron[21,22]. We computed a mean tract model, $R_m$, of all these tracts (**Fig. 3c** and **Supplementary Video 3**). We compared the neurite tracts to $R_m$, at 243 evenly spaced locations. The variability of tract position was 3.26 µm (~5.6 voxels in our images) with a range of 2.1–5.1 µm (**Fig. 3d**).

With ~3-µm variance, BrainAligner produced reliable results. We also differentiated biological variability from aligner variance. The existence of two binary expression systems, *GAL4* and *LexA*[23], permits a rigorous comparison of a computational prediction of overlap with a biological test of 'coexpression'. The *LexA* line (*LexAP036*) showed potential overlap with the *a278-GAL4* line used above in the Ω-shaped antennal lobe commissure (ALC) when registered with BrainAligner (**Fig. 4**). We then expressed distinct reporter constructs using the LexA and *GAL4* systems simultaneously in the same fly and observed overlapping

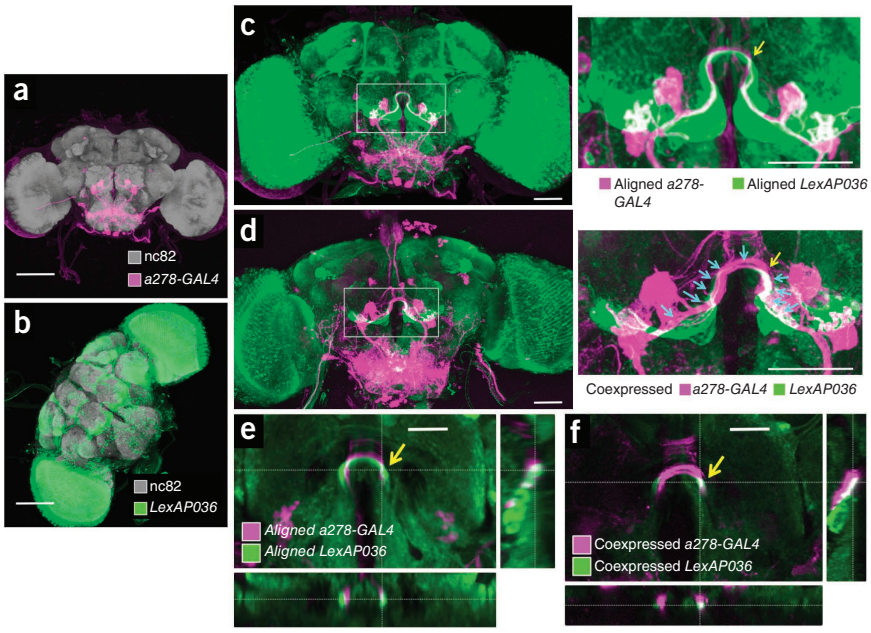


**Figure 4** | Expression pattern overlap by computational and biological methods. (**a**,**b**) Maximum intensity projections of *a278-GAL4;UAS-mCD8-GFP* (**a**) and *LexAP036; lexop-CD2-GFP* (**b**) fly brain slices. (**c**) Aligned image of *GAL4* and LexA expression patterns in **a** and **b**, with close-up views on the right. (**d**) *GAL4* and LexA coexpression patterns, with a close-up view to the right. Blue arrows indicate the 11 locations where overlap of the two patterns was measured, and yellow arrows in **c** and **d** indicate a region of substantial overlap. (**e**,**f**) Cross-sectional views of single slices of the aligned (**e**) and coexpressed (**f**) samples at a position corresponding to the yellow arrow in **c** and **d**. Scale bars, 100 µm (**a**,**b**), 50 µm (**c**,**d**) and 25 µm (**e**,**f**).

expression in the ALC (**Fig. 4d**,**f**). We estimated the precision of BrainAligner's registration using the absolute value of the difference of the biological spatial distance of the two overlapping patterns and their respective spatial distance measured from the computationally aligned patterns. The average distance measured at 11 different spatial locations (**Fig. 4d**) along ALC of the aligned patterns and physically overlapping patterns was 1.8 ± 1.1 µm. Therefore the estimated registration precision was 0.8–2.9 µm. We also saw agreement between the aligned and two-signal images of other GAL4 and LexA pairs with expression patterns in the optic tubercle (**Supplementary Fig. 4** and **Supplementary Videos 4** and **5**).

We independently tested BrainAligner's accuracy by comparing the computational alignment and labeling with both FasII antibody and various *GAL4* lines that express in or near the mushroom bodies. BrainAligner accurately predicted the overlap of FasII antibody staining with the *201Y* and *OK107-GAL4* patterns, but *C232-GAL4*, which is expressed in the central complex, did not localize with FasII (**Fig. 5**).

Finally, the Flp-out technique[24] allows the expression of fluorescent protein reporters in a random subset of neurons in a given *GAL4* expression pattern. Therefore, the computational alignment of Flp-out subsets ('clones') should correlate well with the expression pattern of the parent *GAL4* lines. We aligned the *CG8916-GAL4* expression pattern and Flp-out clones of this *GAL4* line. We observed nested expression patterns in the superior clamp, posterior ventrolateral protocerebrum, anterior ventrolateral protocerebrum, superior lateral protocerebrum and subesophageal ganglion (SOG) (**Supplementary Fig. 5** and **Supplementary Video 6**).

## Building a 3D image atlas of *Drosophila* brain

We automatically registered 2,954 brain images from 470 enhancer trap *GAL4* lines (unpublished data) to our optimized target brain. We selected a well-aligned representative image of each *GAL4* pattern (with $Q_i > 0.5$) and arranged them as a 3D image pattern atlas (**Fig. 1d** and **Supplementary Video 2**). To effectively browse, search and compare the expression patterns in these brains, we developed V3D-AtlasViewer software

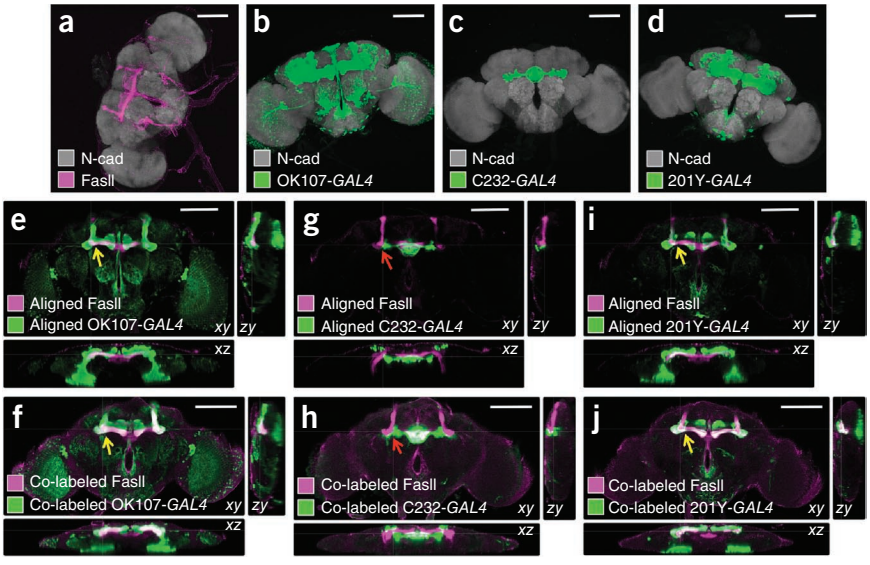


**Figure 5** | Comparison of computational alignment of separate brains with coexpression data in the same brain. (**a**) Confocal image of a wild-type w1118 adult brain labeled with FasII antibody. (**b**–**d**) Expression patterns of the indicated lines shown as maximum intensity projections of 20× confocal image stacks. (**e**–**j**) Cross-sectional views of computational alignments of FasII expression from **a** with *GAL4* patterns from **b**–**d** (**e**,**g**,**i**) and matched cross-sectional views of brains expressing the *GAL4* lines and labeled with both antibodies to GFP and to FasII to show biological overlap (**f**,**h**,**j**). OK107 and 201Y expression patterns overlap with FasII (yellow arrows), but C232 expresses in adjacent but nonoverlapping brain regions (red arrows). In all images, N-cadherin (N-cad) labeling (gray) is the reference signal for alignment to the nc82-labeled target. Magenta, FasII antibody staining; green, *GAL4* expression pattern (staining with antibody to GFP). Scale bars, 100 µm.

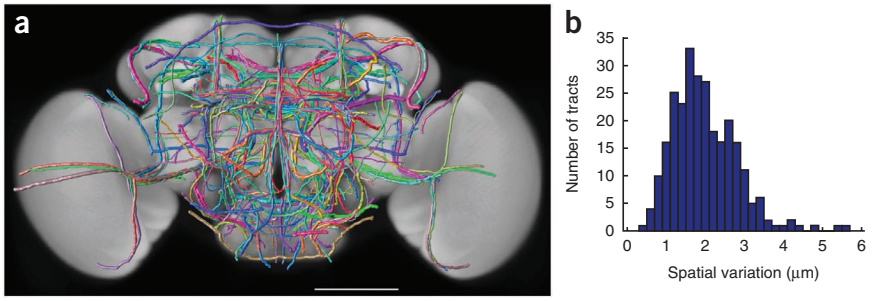


**Figure 6** | A 3D atlas of neurite tracts reconstructed from aligned *GAL4* patterns. (**a**) Distribution of 269 stereotyped randomly colored neurite tracts in the brain. The width of each tract equals the respective spatial deviation. Scale bar, 100 μm. (**b**) Spatial deviation of the neurite tracts.

(**Fig. 1e**) based on our fast 3D image visualization and analysis system V3D[21]. V3D-AtlasViewer organizes the collection of registered *GAL4* patterns using a spreadsheet (**Fig. 1e**), within which a user can select and display any subset of patterns on top of a standard brain for visualization. This 3D image atlas revealed interesting anatomical patterns. For example, visualizing different sections in six *GAL4* patterns demonstrated the previously reported subdivision of the mushroom body horizontal lobe into gamma lobe, beta′ lobe and beta lobe[25] (**Fig. 1f** and **Supplementary Videos 7** and **8**).

With this atlas, to our knowledge for the first time, we analyzed the distribution of *GAL4* patterns in different brain regions in a common coordinate system. The 470 *GAL4* lines covered all known brain compartments (**Supplementary Fig. 6**), with the SOG, superior lateral protocerebrum, prow, mushroom bodies and antennal lobes being the five most represented compartments in this *GAL4* collection. Relatively few *GAL4* lines expressed in superior posterior slope, inferior posterior slope, inferior bridge and gorget. For the central complex of a *Drosophila* brain, less than 20% of *GAL4* lines expressed in the fan-shape body, ellipsoid body and noduli. It may not be surprising that a large fraction of lines expressed in the SOG because this neuropil region represents 7.43% of the brain by volume (**Supplementary Fig. 6**). Therefore we also produced the density map of the neuronal pattern distribution in each compartment, normalizing the distribution by volume (**Supplementary Fig. 6**). The central complex was over-represented in our *GAL4* collection, whereas the SOG, normalized for its volume, was actually underrepresented.

We examined the stereotypy of 269 neurite tracts that project throughout all brain compartments. We reconstructed each tract from at least two aligned brains of each *GAL4* line. We computed the spatial variations and represented them as the width of each tract for visualization (**Fig. 6a** and **Supplementary Video 9**). The average variation was 1.98 ± 0.83 μm (**Fig. 6b**), consistent with our previous independent test of 111 tracts[21]. This range of variation is within the upper bound of biological stereotypy of the neurite tracts themselves and noise introduced in sample preparation, imaging and image analysis including registration and tracing. The tracing error was close to zero[21]. Compared to the typical size of an adult fly brain (590 μm × 340 μm × 120 μm), this small variation indicated strong stereotypy of the neurite tracts.

## DISCUSSION

We used BrainAligner with an optimized virtual target brain, consistent tissue preparation and imaging, and a library of *GAL4* lines, to generate a pilot 3D atlas of neural expression patterns for *Drosophila*. We also applied BrainAligner to our ongoing FlyLight project that will produce an even higher resolution 3D digital map of the *Drosophila* brain. BrainAligner has robustly registered over 17,000 brain images of thousands of *GAL4* lines within a few days, without any manual intervention during the alignment. The ability to align new samples, determined by $Q_i$ scores, is an important quality-control check. We are developing additional methods to expand and query this resource, but it is already in use for anatomical and behavioral investigation of neural circuit principles.

Expression patterns generated by recombinase-based methods to label neurons of a common developmental lineage (mosaic analysis with a repressible cell marker[26]) and images in which single neurons are labeled can be aligned with our *GAL4* reference atlas to identify lines that have *GAL4* expression in those cells, allowing investigation of their behavioral roles. Examination of different *GAL4* expression patterns for proximity or overlap suggests which areas might be functionally connected. The *Drosophila* brain is subdivided into large regions based on divisions in the synaptic neuropil caused by fiber tracts, glial sheaths and cell bodies, but these anatomical regions may be further subdivided by gene expression patterns revealed by the *GAL4* lines. When the *GAL4* lines are aligned to a template brain on which anatomical regions have been labeled, we can annotate the expression patterns using volume image object annotation (VANO) software[27] faster and more uniformly. Alignment permits imaged-based searching, a considerable improvement over keyword searching based on anatomical labels. Accurate alignment of images will also make it easier to correlate anatomy with behavioral consequences. Integration of aligned neuronal patterns with other genetic and physiological screening tools may be used to study different neuron types.

We optimized BrainAligner to run on large datasets of *GAL4* lines expressed in the adult fly brain and ventral nerve cord, but these are not the only type of data that can be aligned. Antibody expression patterns, *in situ* mRNA expression patterns and protein-trap patterns[28,29] are also suitable; if the same reference antibody is included, images from different sources can be aligned using BrainAligner. Although we developed BrainAligner using the nc82 pre-synaptic neuropil marker, we also aligned brains for which the reference channel was generated by staining with rat antibody to N-cadherin (**Fig. 5**). Other reference antibodies that label a more restricted area of the brain, such as FasII antibody, may also work with the algorithm. It is also possible to align any pair of brains directly rather than aligning both to a common template.

BrainAligner can be used in many situations where the image data have different properties than the data presented in this study. The optic lobes of an adult *Drosophila* brain shift in relation to the central brain and distort alignments. We developed an automated method to segregate the optic lobes from the central brain[30], which was then registered using BrainAligner. For the larval nervous system and the adult ventral nerve cord of *Drosophila*, we detected and aligned the principal skeletons of these images[13],

followed by BrainAligner registration. BrainAligner automatically detects the corresponding landmarks, but it permits using manually added landmarks to improve critical alignments or to optimize alignments in a particular brain region. Indeed the brains to be aligned may also be imaged using different magnification scales. Higher-resolution images may have only a part of the brain in the field of view, complicating registration. In such a case, the user can manually supply as few as four to five markers using V3D software[21] to generate a globally aligned brain, which can then be automatically aligned using BrainAligner.

Despite several successfully used image registration methods in other scenarios such as building the Allen mouse brain atlas[10], we have not found another automated image registration method that performs as well as BrainAligner on our large-scale applications. Indeed, the key algorithm in BrainAligner, the RLM method, can be viewed as an optimized combination of several existing methods. It compares the results produced using different criteria and only uses results that agree with each other. BrainAligner is not limited to fruit fly brains and could be applied to other image data such as mouse brains.

## METHODS

Methods and any associated references are available in the online version of the paper at http://www.nature.com/naturemethods/.

*Note: Supplementary information is available on the Nature Methods website.*


### ACKNOWLEDGMENTS

We thank G. Rubin, B. Pfeiffer and K. Hibbard (Janelia Farm Research Campus, Howard Hughes Medical Institute) for the *pJFRC21-10XUAS-IVS-mCD8::RFP, lexAop-CD2-GFP* stock and *LexAP* vector; B. Ganetzky for collaboration in generating the *GAL4* collection; B. Lam for visually scoring the quality of aligned brains; Y. Zhuang for tracing and proofreading neurite tracts; Y. Yu and J. Yang for manual landmarking; C. Zugates and members of the FlyLight project team for discussion of aligner optimization; G. Wu for help in testing a registration method; D. Shen for discussion when we initially developed BrainAligner; and G. Rubin for commenting on this manuscript. This work was funded by Howard Hughes Medical Institute.


### AUTHOR CONTRIBUTIONS

H.P. designed and implemented BrainAligner, and performed experiments and analyses. H.P. and J.H.S. designed the biological experiments. F.L. and E.W.M. helped design the algorithm. P.C. prepared the samples and acquired confocal images. L.Q. helped implement the random sample consensus algorithm and some comparison experiments. A.J. produced the brain compartment label field. A.M.S. and J.H.S. generated *LexA* lines. H.P., E.W.M. and J.H.S. wrote the manuscript.

### COMPETING FINANCIAL INTERESTS

The authors declare no competing financial interests.


**Published online at http://www.nature.com/naturemethods/.**
**Reprints and permissions information is available online at http://www.nature.com/reprints/index.html.**



1. Buchner, E. *et al.* Cell-specific immuno-probes for the brain of normal and mutant *Drosophila melanogaster*. I. Wildtype visual system. *Cell Tissue Res.* **253**, 357–370 (1988).
2. Brand, A.H. & Perrimon, N. Targeted gene expression as a means of altering cell fates and generating dominant phenotypes. *Development* **118**, 401–415 (1993).
3. Luan, H. & White, B.H. Combinatorial methods for refined neuronal gene targeting. *Curr. Opin. Neurobiol.* **17**, 572–580 (2007).
4. Broughton, S.J., Kitamoto, T. & Greenspan, R.J. Excitatory and inhibitory switches for courtship in the brain of *Drosophila melanogaster*. *Curr. Biol.* **14**, 538–547 (2004).
5. Jenett, A., Schindelin, J.E. & Heisenberg, M. The Virtual Insect Brain protocol: creating and comparing standardized neuroanatomy. *BMC Bioinformatics* **7**, 544 (2006).
6. Boerner, J. & Duch, C. Average shape standard atlas for the adult *Drosophila* ventral nerve cord. *J. Comp. Neurol.* **518**, 2437–2455 (2010).
7. Maintz, J.B.A. & Viergever, M.A. A survey of medical image registration. *Med. Image Anal.* **2**, 1–36 (1998).
8. Zitova, B. & Flusser, J. Image registration methods: a survey. *Image Vis. Comput.* **21**, 977–1000 (2003).
9. Fischer, B., Dawant, B. & Lorenz, C. (eds.) *Biomedical Image Registration*, Proceedings of the 4th International Workshop (Springer, 2010).
10. Lein, E.S. *et al.* Genome-wide atlas of gene expression in the adult mouse brain. *Nature* **445**, 168–176 (2007).
11. Jefferis, G.S. *et al.* Comprehensive maps of *Drosophila* higher olfactory centers: spatially segregated fruit and pheromone representation. *Cell* **128**, 1187–1203 (2007).
12. Chiang, A.S. *et al.* Three-dimensional reconstruction of brain-wide wiring networks in *Drosophila* at single-cell resolution. *Curr. Biol.* **21**, 1–11 (2011).
13. Qu, L. & Peng, H. A principal skeleton algorithm for standardizing confocal images of fruit fly nervous systems. *Bioinformatics* **26**, 1091–1097 (2010).
14. Thirion, J.P. Image matching as a diffusion process: an analogy with Maxwell's demons. *Med. Image Anal.* **2**, 243–260 (1998).
15. Shen, D. & Davatzikos, C. HAMMER: hierarchical attribute matching mechanism for elastic registration. *IEEE Trans. Med. Imaging* **21**, 1421–1439 (2002).
16. Vercauteren, T. & Pennec, X. Perchant, A. & Ayache, N. Symmetric log-domain diffeomorphic registration: a demons-based approach. *Lect. Notes Comput. Sci.* **5241**, 754–761 (2008).
17. Wagh, D.A. *et al.* Bruchpilot, a protein with homology to ELKS/CAST, is required for structural integrity and function of synaptic active zones in *Drosophila*. *Neuron* **49**, 833–844 (2006).
18. Maes, F., Collignon, A., Vandermeulen, D., Marchal, G. & Suetens, P. Multimodality image registration by maximization of mutual information. *IEEE Trans. Med. Imaging* **16**, 187–198 (1997).
19. Fischler, M.A. & Bolles, R.C. Random sample consensus: a paradigm for model fitting with applications to image analysis and automated cartography. *Commun. ACM* **24**, 381–395 (1981).
20. Bookstein, F.L. Principal warps: thin-plate spline and the decomposition. *IEEE Trans. Pattern Anal. Mach. Intell.* **11**, 567–585 (1989).
21. Peng, H., Ruan, Z., Long, F., Simpson, J.H. & Myers, E.W. V3D enables real-time 3D visualization and quantitative analysis of large-scale biological image data sets. *Nat. Biotechnol.* **28**, 348–353 (2010).
22. Peng, H., Ruan, Z., Atasoy, D. & Sternson, S. Automatic reconstruction of 3D neuron structures using a graph-augmented deformable model. *Bioinformatics* **26**, i38–i46 (2010).
23. Lai, S.L. & Lee, T. Genetic mosaic with dual binary transcriptional systems in *Drosophila*. *Nat. Neurosci.* **9**, 703–709 (2006).
24. Basler, K. & Struhl, G. Compartment boundaries and the control of *Drosophila* limb pattern by hedgehog protein. *Nature* **368**, 208–214 (1994).
25. Crittenden, J.R., Skoulakis, E., Han, K., Kalderon, D. & Davis, R.L. Tripartite mushroom body architecture revealed by antigenic markers. *Learn. Mem.* **5**, 38–51 (1998).
26. Lee, T. & Luo, L. Mosaic analysis with a repressible cell marker for studies of gene function in neuronal morphogenesis. *Neuron* **22**, 451–461 (1999).
27. Peng, H., Long, F. & Myers, E.W. VANO: a volume-object image annotation system. *Bioinformatics* **25**, 695–697 (2009).
28. Kelso, R.J. *et al.* Flytrap, a database documenting a GFP protein-trap insertion screen in *Drosophila melanogaster*. *Nucleic Acids Res.* **32**, D418–D420 (2004).
29. Knowles-Barley, S., Longair, M. & Douglas, A.J. BrainTrap: a database of 3D protein expression patterns in the *Drosophila* brain. *Database* 10.1093/database/baq005 (2010).
30. Lam, S.C. *et al.* Segmentation of center brains and optic lobes in 3D confocal images of adult fruit fly brains. *Methods* **50**, 63–69 (2010).

## ONLINE METHODS

**Immunohistochemistry and confocal imaging.** Males from *enhancer-GAL4* lines (unpublished data, J.H.S. and B. Ganetzky) were crossed to virgin *UAS-mCD8-GFP* (Bloomington #5137; ref. 26) that produces a membrane-targeted fluorescent protein in the neurons. Adult brains were dissected in PBS (pH 7), fixed overnight in 2% paraformaldehyde, washed extensively in PBS with 0.5% Triton and then incubated overnight at 4 °C rotating in primary antibodies nc82 (1:50 Developmental Studies Hybridoma Bank[17]) and rabbit anti-GFP (1:500 Molecular Probes/Invitrogen A11122). After washing all day at room temperature (~21 °C), brains were incubated overnight at 4 °C rotating with secondary antibodies: goat anti-mouse–Alexa Fluor 568 and goat anti-rabbit–Alexa Fluor 488 (1:500; Molecular Probes/Invitrogen; A11034 and A11031, respectively). After another day of washing, brains were cleared and mounted in the glycerol-based Vectashield (on glass slides with two clear reinforcement rings as spacers (Avery). Samples were imaged on Zeiss Pascal Confocal microscope with 0.84 µm *z*-dimension steps using a 20× air-immersion lens. Sequential scanning was used to ensure that there was no bleed-through between the reference and pattern channels. The raw images collected had 1,024 × 1,024 × *N* voxels (number of *z*-dimension sections, *N*, typically was around 160), 8 bits (voxel size = 0.58 µm × 0.58 µm × 0.84 µm) and two color channels. The gain was increased as the imaging depth increased to maintain optimal use of detector range; the pattern channel intensity was maintained between over- and undersaturation. This resulted in a gain ramp of roughly 10% from lens-proximal to lens-distal surface of sample.

The *enhancer-LexA* lines (A.M.S. and J.H.S., unpublished data) were crossed to *LexOp-CD2-GFP* (in *attP2* generated by A.M.S.) and stained with nc82 and anti-GFP as described above. For the double-label experiments, combination stocks of *LexOp-CD2-GFP*, pJFRC21-10XUAS-IVS-mCD8::RFP; *enhancer-GAL4*[31,32] were built and crossed to the *LexA* lines. These lines were stained with rabbit anti-GFP (1:500) and rat anti-CD8 (1:400; Invitrogen). The secondary antibodies were Alexa Fluor 488–labeled anti-rabbit and Alexa Fluor 568–labeled anti-rat (1:500). For the Flp-out clones, *GAL4* lines were crossed to *hs-Flp; UAS-FRT-CD2-FRT-mCD8-GFP* stocks[33] and heat-shocked at the end of embryonic development or in adulthood.

Other fly stocks, *C232-GAL4* (ref. 34), *201Y-GAL4* (ref. 35) and *OK107-GAL4* (ref. 36), were obtained from the Bloomington Stock Center. Other antibodies used were to FasII[37] (1D4; 1:50) and to N-cadherin[38] (DNEX#8; 1:50), both from the Developmental Studies Hybridoma Bank (developed under the auspices of the US National Institute of Child Health and Human Development and maintained by The University of Iowa, Iowa City, Department of Biology).

**BrainAligner implementation.** To maximize the robustness of the automatic alignment and avoid being entrapped in local minima, in BrainAligner we used sequential global affine alignment in three steps. First we aligned the center of mass of a subject image to that of the target image. Then we rescaled a subject image proportionally so that its principal axis (obtained via principal component analysis) had the same length with that of the target image. Finally, we rotated a subject image around its center of mass and thus detected the angle for which the target image and the rotated subject image had the greatest overlap. As normally we did not have shearing in the 3D images, we did not optimize it for the affine transform. The rescaling step might also be skipped as brains imaged under the same microscope setting had similar size.

For the local nonlinear alignment, we computed the features based on adaptively determined image patches. The radius of an image patch was calculated using the formula $48 \times S/512$, in which $S$ is the largest image dimension in three dimensions. To reduce the computational complexity, we searched matching landmarks hierarchically, first at a coarse level (grid spacing of 16 voxels) and then at a fine level (grid spacing of 1 voxel) around the best matching location (within a 13 voxel × 13 voxel × 7 voxel window) detected at a coarse level. The mutual information was calculated on discretized image voxel intensity, by binning the grayscale intensity into 16 evenly spaced intensity levels. For the random sample consensus (RANSAC) step, we implemented the constraint that all matching landmark pairs would satisfy a global affine transformation. Thus we computed the Euclidian distances of all initial matching landmark pairs after such a transformation and removed the matching pairs that had more than two times the s.d. of the distance distribution.

We designed a fast way to compute the thin-plate-spline[20] (TPS)-based displacement field, which was used to warp images. We computed the displacement field using TPS for a sub-grid (with 4 voxel × 4 voxel × 4 voxel downsampling) of an entire image, followed by tri-linear interpolation for all remaining voxels to approximate the entire TPS transform. This method resulted in very similar displacement field compared to a direct implementation of TPS but is about 50 times faster.

**Data analyses.** For the co-localization analysis using co-expressed *GAL4* and *LexA* patterns, we measured distances between a series of pairs of high-curvature locations along the respective co-expressed *GAL4* and *LexA* patterns in the ALC tract. We treated these distances as the ground truth of characteristic features that should be matched in computationally aligned brains. Then in the aligned brains, we visually detected these matching locations and produced the respective distance measurements. The error of registration was defined as the absolute value of the difference between the corresponding distances.

The correlation analysis for the Flp-out data was performed around each of the co-localized subset clone patterns and the parent pattern. We first used V3D-Neuron[21] to trace the co-localized neurite tracts, which were used to define the 'foreground' image region of interest for the correlation analysis. Suppose a foreground region of interest had $K$ voxels, then we randomly sampled another $K$ voxels from the remaining brain area as the negative control for calculating the correlation coefficient for this co-localized subset clone pattern and the parent pattern.

In the analysis of *GAL4* pattern distribution, for an aligned brain image, we calculated the mean value, $m$, and s.d. ($\sigma$) of the entire brain area. We defined a brain compartment as having neuronal pattern(s) if (i) it had any absolutely visible voxels (typically intensity > 50 for an 8-bit image) and (ii) its voxel intensities were outstanding compared to the average expression signal in the entire brain area (that is, intensity > $m + 3 \times \sigma$). The names of brain compartments we used are consistent with the ongoing effort of an international fruit fly brain nomenclature group.

**Data and software.** The BrainAligner and V3D-AtlasViewer software are available as **Supplementary Software 1**. BrainAligner, the optimized target brain as well as additional information about BrainAligner, can also be downloaded from http://penglab.janelia.org/proj/brainaligner/. The V3D AtlasViewer program is a module of V3D[21], which can be freely downloaded from http://penglab.janelia.org/proj/v3d/. Atlas files and representative confocal images are available on request.


31. Pfeiffer, B.D. *et al.* Refinement of tools for targeted gene expression in *Drosophila*. *Genetics* **186**, 735–755 (2010).
32. Pfeiffer, B.D. *et al.* Tools for neuroanatomy and neurogenetics in *Drosophila*. *Proc. Natl. Acad. Sci. USA* **105**, 9715–9720 (2008).
33. Wong, A.M., Wang, J.W. & Axel, R. Spatial representation of the glomerular map in the *Drosophila* protocerebrum. *Cell* **109**, 229–241 (2002).
34. O'Dell, K.M.C., Armstrong, J.D., Yang, M.Y. & Kaiser, K. Functional dissection of the *Drosophila* mushroom bodies by selective feminization of genetically defined subcompartments. *Neuron* **15**, 55–61 (1995).
35. Yang, M.Y., Armstrong, J.D., Vilinsky, I., Strausfeld, N.J. & Kaiser, K. Subdivision of the *Drosophila* mushroom bodies by enhancer-trap expression patterns. *Neuron* **15**, 45–54 (1995).
36. Connolly, J.B. *et al.* Associative learning disrupted by impaired Gs signaling in *Drosophila* mushroom bodies. *Science* **274**, 2104–2107 (1996).
37. Grenningloh, G., Rehm, E.J. & Goodman, C.S. Genetic analysis of growth cone guidance in *Drosophila*: fasciclin II functions as a neuronal recognition molecule. *Cell* **67**, 45–57 (1991).
38. Iwai, Y. *et al.* Axon patterning requires DN-cadherin, a novel adhesion receptor, in the *Drosophila* embryonic CNS. *Neuron* **19**, 77–89 (1997).






doi:10.1038/nmeth.1602